# Simulation study of stepwise relaxation in a spheromak plasma

Ritoku Horiuchi and Tetsuya Sato
*National Institute for Fusion Science, Nagoya 464-01, Japan*

Masaya Uchida
*Faculty of Engineering, Osaka University, Suita 565, Japan*

(Received 16 September 1991; accepted 18 November 1991)

The energy relaxation process of a spheromak plasma in a flux conserver is investigated by means of a three-dimensional magnetohydrodynamic simulation. The resistive decay of an initial force-free profile brings the spheromak plasma to an $m = 1/n = 2$ ideal kink unstable region. It is found that the energy relaxation takes place in two steps; namely, the relaxation consists of two physically distinguished phases, and there exists an intermediate phase in between, during which the relaxation becomes inactive temporarily. The first relaxation corresponds to the transition from an axially symmetric force-free state to a helically symmetric one with an $n = 2$ crescent magnetic island structure via the helical kink instability. The $n = 2$ helical structure is nonlinearly sustained in the intermediate phase. The helical twisting of the flux tube creates a reconnection current in the vicinity of the geometrical axis. The second relaxation is triggered by the rapid growth of the $n = 1$ mode when the reconnection current exceeds a critical value. The helical twisting relaxes through magnetic reconnection toward an axially symmetric force-free state. It is also found that the poloidal flux reduces during the helical twisting in the first relaxation and the generation of the toroidal flux occurs through the magnetic reconnection process in the second relaxation.

## I. INTRODUCTION

The energy relaxation process in a plasma system with two different time scales is an attractive topic not only from the standpoint of controlled nuclear fusion but also from the standpoint of nonlinear plasma physics. For instance, a magnetically confined magnetohydrodynamic (MHD) plasma self-organizes to the minimum energy state in the system where two physical processes are operative, i.e., driven magnetic reconnection as a fast process and resistive diffusion as a slow process.[1] Both the topological change of a global magnetic confinement configuration and the dissipation of an excess free magnetic energy, which can take place only in the resistive medium, are brought about by the driven reconnection in a fast time scale comparable to the MHD time scale.[1,2] The sawtooth oscillation in the tokamak plasma is also another relaxation phenomenon in which two phenomena with different time scales, i.e., the slow ramp-up and the fast crash, take place reciprocally.[3]

The spheromak configuration is one of the compact tori in which the poloidal and toroidal fields are sustained by the internal plasma current. It is widely known that the minimum energy state in the low-beta plasma is the force-free state with a constant coefficient, what is called the Taylor state.[4] The experimentally formed spheromak plasma has a configuration very close to the Taylor state.[5] If the resistivity, however, has a spatial dependence, the current profile is modified in the resistive diffusion time scale and thus the plasma gradually leaves from the Taylor state. The deviation from the minimum energy state makes the system unstable and excites a kind of relaxation instability.

There are two kinds of dangerous instabilities in the spheromak plasma. The first one is a global MHD instability such as shift or tilt mode which occurs in the free boundary case.[6,7] These modes are found to be stabilized by confining the plasma in the oblate flux conserver.[6-8] The second one is a relaxation instability in a flux conserver, which takes place as a result of resistive decay of an initial stable profile. The stepwise decay of the magnetic field strength was often observed in the relaxation instability.[9,10] From the analysis of the experimental data[9] and the numerical studies,[11-13] the stepwise relaxation is believed to be triggered by the excitation of the $n = 2$ ideal kink mode when the stable profile with a minimum energy changes to a low-$q$ profile of $q < 0.5$, where $n$ is a toroidal mode number and $q$ is the safety factor.

Sgro *et al.*[11] have examined the stepwise relaxation by using a two-dimensional transport code for a current peaking phase and a three-dimensional nonlinear MHD code for a dynamical evolution phase. They found that a nonlinear saturation state appeared after the excitation of the $n = 2$ kink mode and that the axisymmetric force-free state was realized again through the experience of this intermediate state. Katayama and Katsurai[12] and Ono and Katsurai[13] have also examined the relaxation process in spheromak plasmas with a high-$q$ profile and a low-$q$ profile by means of the MHD simulation. They introduced several assumptions and numerical techniques to obtain a numerically stable solution, but some of them were not appropriate for an analysis of the stepwise relaxation phenomenon. Especially, as will be discussed in this paper, it is quite important to describe the magnetic reconnection process with a sufficiently high accuracy in the vicinity of the geometrical axis in order to reveal the physical process in a self-consistent way.

In order to improve the numerical accuracy we developed a new numerical scheme which relies on the explicit finite-difference method with fourth-order accuracy both in space and time.[14] This scheme enables us to simulate a physical phenomenon over the resistive diffusion time scale with a sufficiently high accuracy by reducing to a much lower level the accumulation of the numerical error that comes

 0899-8221/92/030672-11$04.00  

from the finite-difference method. This scheme has succeeded in describing several nonlinear phenomena in fusion[14,15] and space plasmas.[16]

The purpose of this paper is to examine the whole relaxation process from an initial current peaking phase through the final force-free state by using the three-dimensional full MHD simulation and to clarify the physical mechanism of the stepwise relaxation in a spheromak plasma. For this we restrict the discussion to the relaxation phenomenon in a spheromak plasma with a low-$q$ profile that is considered to show the stepwise relaxation as a result of the resistive decay. The initial condition and the simulation model are described in Sec. II. Section III is devoted to discussions on a new physical picture of the stepwise relaxation based on the detailed analysis of the results obtained from the MHD simulation and to comparisons with experimental results and other numerical simulation results. Finally we give a summary of this paper and a brief discussion on the applicability of the model in Sec. IV.

## II. SIMULATION MODEL

We study the relaxation process of a low-beta spheromak plasma in a flux conserver by making use of three-dimensional MHD simulation. The numerical scheme used for simulation relies on the explicit finite-difference method with fourth-order accuracy both in space and time.[14] The equations to be solved are the resistive, nonlinear MHD equations,

$$\frac{\partial \rho}{\partial t} = -\nabla\cdot(\rho \mathbf{v}), \tag{1}$$

$$\frac{\partial \mathbf{F}}{\partial t} = -\nabla\cdot(\mathbf{F}\mathbf{v}) - \nabla p + \mathbf{j}\times\mathbf{B}, \tag{2}$$

$$\frac{\partial \mathbf{B}}{\partial t} = \nabla\times(\mathbf{v}\times\mathbf{B} - \eta\mathbf{j}), \tag{3}$$

$$\frac{\partial p}{\partial t} = -\nabla\cdot(p\mathbf{v}) + (\gamma-1)(-p\nabla\cdot\mathbf{v} + \eta\mathbf{j}\cdot\mathbf{j}), \tag{4}$$

where

$$\mathbf{j} = \nabla\times\mathbf{B}, \tag{5}$$

and $\mathbf{F}(=\rho\mathbf{v})$ is the mass flux density, $p$ is the thermal pressure, $\rho$ is the matter density, $\mathbf{v}$ is the matter velocity, $\mathbf{B}$ is the magnetic field, $\mathbf{j}$ is the current density, $\eta$ is the electrical resistivity, and $\gamma(=5/3)$ is the ratio of specific heats.

The shape of the flux conserver is assumed to be an ellipsoid of revolution with the aspect ratio of $z_{fc}/r_{fc} = 0.6$ in the cylindrical coordinates $(r,\phi,z)$, where the symmetric axis is taken to be along the $z$ axis, $z_{fc}$ is the half-length along the $z$ axis, and $r_{fc}$ is the radius in the midplane $(z=0)$. We adopt the configuration of the CTCC-I device[9] as a simulation model. The oblate shape plays a role in protecting the plasma from disruptive growing of the external tilt mode.[6-8] The simulation domain is implemented on a $(75\times16\times91)$ point grid with fixed separations $(\Delta r,\Delta\phi,\Delta z)$ in the cylindrical coordinates. The boundary condition to be imposed is such that $\mathbf{B}\cdot\mathbf{n}=0$, $\mathbf{j}\times\mathbf{n}=0$, and $\mathbf{v}=0$ on the conducting wall, where $\mathbf{n}$ is the unit vector normal to the boundary surface. Because there are no spatial grids on the boundary surface in general, we impose the boundary condition on the spatial grids located one grid space ($\Delta r$ or $\Delta z$) inside from the boundary surface. This replacement is equivalent to the modification of the boundary shape.

In order to obtain the initial condition we solve two-dimensional Grad–Shafranov equation numerically[17] by assuming the poloidal current and thermal pressure profiles as

$$I(\psi) = I_0\Psi^{\alpha}, \tag{6}$$

$$p(\psi) = p_0\Psi^{\beta}, \tag{7}$$

where

$$\Psi = [\psi_h - \psi(r,z)]/(\psi_h - \psi_0), \tag{8}$$

$\psi(r,z)$ is the poloidal flux function, $\psi_0$ is the value at a magnetic axis, $\psi_h$ is the value at a plasma–vacuum boundary, and $\alpha$ and $\beta$ are constant parameters. Figure 1 shows the contour plots of the poloidal flux function for the case where there is 0.1 of the total poloidal flux in the vacuum region $(\psi_h/\psi_0 = 0.1)$, $\alpha = 1.1$, and $p_0 = 0$. The solution is chosen so that the magnetic separatrix coincides with the ellipsoidal boundary and the safety factor on the magnetic axis $q_{axis}$ is a little larger than 0.5 to keep the system stable against the $m = 1/n = 2$ kink instability. Here $m$ and $n$ are the poloidal and toroidal mode numbers, respectively. This solution is not exactly equal, but very close, to the Taylor state with the minimum energy, which is given by setting $p_0 = 0$ and $\alpha = 1.0$.

We consider two types of resistivity with spatially hollow profiles, both of which are described by the following relation:

$$\eta(r,z) = \eta_v + (\eta_p - \eta_v)(3X^2 - 2X^3), \tag{9}$$

where $X(r,z)$ is the function satisfying the relation $0\leqslant X\leqslant 1$, and $\eta_v$ and $\eta_p\,(<\eta_v)$ are the values of the resistivity in the vacuum region $(X=0)$ and at the plasma center $(X=1)$, respectively. The functional dependence of $\eta$ is determined so that the gradient vanishes both in the vacuum region and at the plasma center. It is reasonable to assume that the resistivity has a relatively smaller value in the hot central region compared with that in the cold periphery region. The first type corresponds to the torus profile case where the function $X(r,z)$ is given by $j_\phi/j_{\phi,\max}$ [$j_\phi(r,z)$ is the $\phi$ component of the initial current density and $j_{\phi,\max}$ is its maximum value]. The second type corresponds to the ellipsoid profile case where

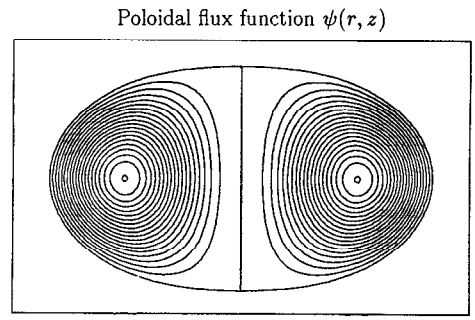


FIG. 1. Contour map of the poloidal flux function in the poloidal plane for the two-dimensional equilibrium solution when there is 0.1 of the total poloidal flux in the vacuum region $(\psi_h/\psi_0 = 0.1)$, $\alpha = 1.1$, and $p_0 = 0$.

the function $X(r,z)$ is equal to $\sqrt{1-[(r/r_{fc})^2+(z/z_{fc})^2]}$. Figure 2 shows the spatial distribution of the resistivity in the poloidal plane for the torus profile case (top) and that for the ellipsoid profile case (bottom). The resistivity profile is fixed to the initial one throughout the simulation run because it is very difficult to obtain the resistivity profile corresponding to the temporal change of the physical parameters. The perturbations of the velocity field are assigned by random numbers on each grid point, the maximum amplitude of which is equal to $10^{-3}$ of the average Alfvén velocity $v_{A0}$.

## III. SIMULATION RESULTS

Four simulation runs are carried out under the assumption that the plasma pressure is negligibly small ($p \ll \mathbf{B}\cdot\mathbf{B}$) and the matter density is spatially uniform. The simulation parameters are listed in Table I, where the period and the resistivity are normalized by the Alfvén transit time ($\equiv r_{fc}/v_{A0}$) and $r_{fc}v_{A0}$, respectively. The simulation run starts from the force-free equilibrium of $q_{axis}=0.524$ and is terminated after the duration of $150t_A$ for case A. The simulation runs B, C, and D are carried out to examine the dependence on the spatial profile of the resistivity and the dependence on the toroidal mode number where the simulation data at $t=80t_A$ for case A are used as initial data. We devote ourselves to the analysis of the simulation result for case A in the following unless otherwise stated.

### A. Stepwise relaxation

Figure 3 shows the temporal evolutions of the total magnetic energy (solid line), the $n=2$ mode amplitudes of the magnetic field (dashed line), and the flow velocity (dotted line) where these quantities are normalized by their maximum values. There are two peaks in the mode curve of the flow velocity while there is one trapezoidal hill in the mode curve of the magnetic field. The energy relaxation takes place stepwise at the periods corresponding to the peaks of the $n=2$ flow mode. Let us analyze the stepwise relaxation phenomenon by separating the temporal evolution into four typical phases, i.e., the linear phase, the first relaxation phase, the nonlinear saturation phase, and the second relaxation phase. Both the $n=2$ flow mode and the $n=2$ magnetic field mode grow with the same growth rate in the linear phase where the mode amplitude of the perturbed field is much smaller than the unperturbed magnetic field ($23t_A < t < 80t_A$). In the first relaxation phase the growth curve of the $n=2$ flow mode attains the first peak and the resultant deformation of the equilibrium profile leads to rapid dissipation of the magnetic energy ($80t_A < t < 100t_A$). In the nonlinear saturation phase which follows the first relaxation phase, the mass flow energy is relaxed to some lower level, while the $n=2$ structure of the magnetic field is nonlinearly sustained ($100t_A < t < 120t_A$). The $n=2$ magnetic energy rapidly dissipates and the $n=2$ flow mode grows to the maximum level in the second relaxation phase ($120t_A < t < 140t_A$).

Let us then examine the behaviors of physical quantities in the linear phase in detail. Because the resistivity has a larger value in the periphery region than that in the central region, the resistive diffusion proceeds so that the toroidal

TABLE I. Simulation parameters. The columns of "type" and "mode" show the type of resistivity profile defined by Eq. (9) and the toroidal mode number excluded from the simulation, respectively. The column of "period" represents the simulation period in units of the Alfvén transit time.

| Case | Type | Period | $\eta_p$ | $\eta_v$ | Mode |
|---|---|---|---|---|---|
| A | torus | $0<t<150$ | $2\times10^{-6}$ | $1\times10^{-4}$ | no |
| B | ellipsoid | $80<t<150$ | $2\times10^{-6}$ | $1\times10^{-4}$ | no |
| C | torus | $80<t<150$ | $2\times10^{-6}$ | $1\times10^{-4}$ | $n=3$ |
| D | torus | $80<t<150$ | $2\times10^{-6}$ | $1\times10^{-4}$ | $n=1$ |

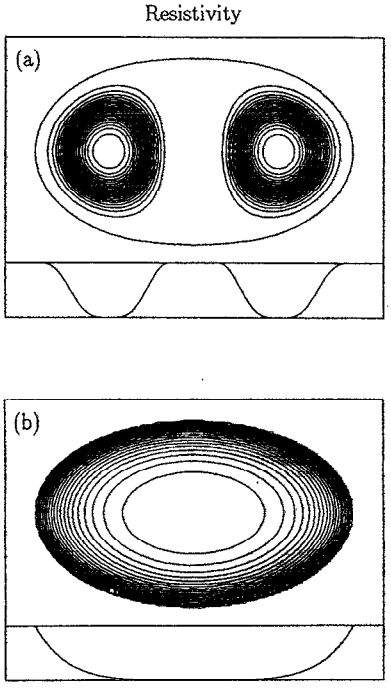


FIG. 2. Spatial distributions of the resistivity in the poloidal plane for (a) the torus profile case, and (b) the ellipsoid profile case.

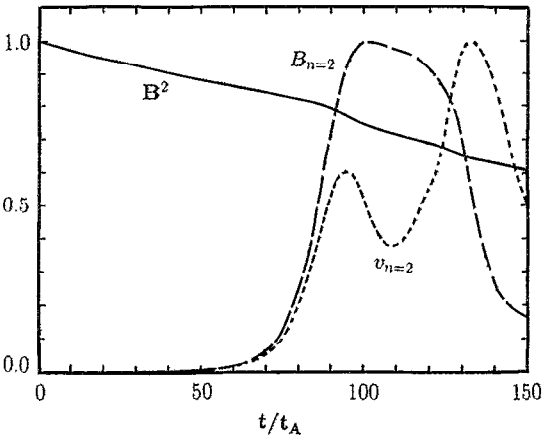


FIG. 3. Temporal evolutions of the total magnetic energy (solid line), the $n=2$ mode amplitudes of the magnetic field (dashed line), and the flow velocity (dotted line) for case A where these quantities are normalized by their maximum values.

current concentrates in the vicinity of the magnetic axis. The peaking of the toroidal current results directly in the decrease of the safety factor. Figure 4 shows the temporal evolutions of $q_{\text{axis}}$ (solid line), and the mode amplitudes of the $n = 1$ mode (dashed line), the $n = 2$ mode (dotted line), and the $n = 3$ mode (dot-dashed line) where the mode amplitude is plotted in the logarithmic scale attached to the left vertical axis, while the safety factor is plotted in a linear scale attached to the right vertical axis. The value of $q_{\text{axis}}$ decreases monotonously with time until it reaches the minimum value of $q_{\text{axis}} = 0.438$ at $t \approx 79t_A$. The magnetic configuration changes in the resistive diffusion time scale determined by the vacuum resistivity in the linear phase. Notice in Fig. 4 that the $n = 2$ mode starts to grow soon after $q_{\text{axis}}$ decreases below 0.5, while both the $n = 1$ mode and the $n = 3$ mode remain almost unchanged. This indicates the fact that the $m = 1/n = 2$ ideal kink instability is triggered at the period ($t \approx 23t_A$) when the field configuration satisfies the condition $q(r,z) < 0.5$ everywhere.[11] The growth rate of the kink instability is estimated to be nearly equal to $0.13/t_A$ from the inclination of the growth curve.

The safety factor $q_{\text{axis}}$ begins to increase after it reaches the minimum value ($t \geqslant 80t_A$). The growth rate of the kink mode becomes smaller as the system approaches the nonlinear state. Let us examine the behavior of the $n = 2$ mode in the nonlinear phase. The Poincaré plots of magnetic field lines on the poloidal plane ($\phi = 0$) are displayed in Fig. 5 at six different times where six panels correspond to the Poincaré plots at $t = 0$, $90t_A$, $105t_A$, $115t_A$, $120t_A$, and $135t_A$, respectively. The $m = 1/n = 2$ plasma flow created by the instability gradually modifies the magnetic surface so that the location of the magnetic axis is helically shifted from the axially symmetric point ($t = 90t_A$). The magnetic islands appear around the magnetic axis as a result of nonlinear mode coupling. Further deformation leads to overlapping of the magnetic islands which changes the ordered magnetic structure with nicely nested magnetic surfaces to the chaotic one ($t = 105t_A$). The remaining magnetic surfaces tend to deform into crescent shapes as the magnetic axis approaches

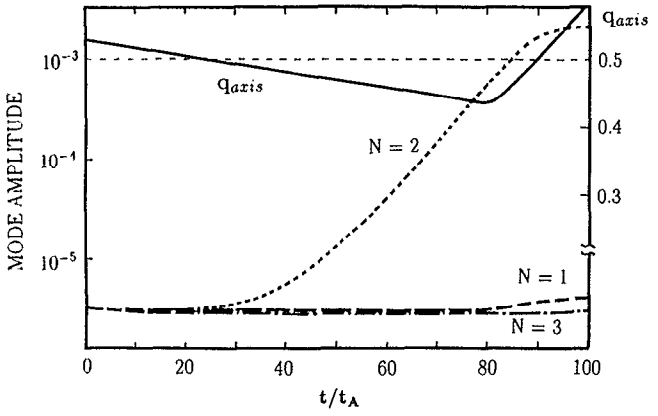


FIG. 4. Temporal evolutions of $q_{\text{axis}}$ (solid line), and the mode amplitudes of the $n = 1$ mode (dashed line), the $n = 2$ mode (dotted line), and the $n = 3$ mode (dot-dashed line) for case A where the mode amplitude is plotted in the logarithmic scale attached to the left vertical axis, while the safety factor is plotted in a linear scale attached to the right vertical axis.

the periphery region. In this process the hot core plasma is carried from the central region to the cold periphery region with a relatively large resistivity. This movement results in rapid dissipation of the magnetic energy in the first relaxation phase. The dynamical deformation is stopped because the $n = 2$ flow mode ceases to grow and decays to some lower level at this stage. On the other hand, the $n = 2$ helical structure of the magnetic field shown in Fig. 5 is quasistationarily sustained for a duration of about $20t_A$. This corresponds to the fact that the $n = 2$ mode of the magnetic field keeps its amplitude almost unchanged in the nonlinear phase (see Fig. 3). As soon as the second relaxation starts, a new magnetic axis appears in the chaotic region ($t = 120t_A$). This is because the high-$m$ modes in the chaotic region dissipates rapidly and the low-$m$ structure appears. While increasing the area of the new well-organized magnetic surface, the magnetic axis moves toward the axially symmetric position. This implies that the $n = 2$ mode of the magnetic field decays at this stage. In this way the axisymmetric profile is realized again in the plasma after the stepwise relaxation.

The second relaxation is followed by the topological change of the magnetic field from the $n = 2$ helical configuration to the axisymmetric configuration. The topological change is completed by the operation of magnetic reconnection in the MHD plasma. In order to clarify the transition mechanism, let us examine the three-dimensional structure of the magnetic field line. Figure 6 shows three-dimensional display of the magnetic field line at $t = 0$ (left top), $t = 90t_A$ (left bottom), $t = 100t_A$ (right top), and $t = 135t_A$ (right bottom). The initial axisymmetric configuration is gradually deformed by the growth of the $m = 1/n = 2$ helical kink mode ($t = 90t_A$). The deformation proceeds in such a way that the flux tube is helically twisted as a whole ($t = 100t_A$). The helical twisting concentrates the magnetic flux in the vicinity of the geometrical axis ($r = 0$). Because the magnetic field on one side of the twisted tube contacts obliquely with that on the opposite side at the geometrical axis, the reconnection current along the $z$ axis is formed at the contact point. Figure 7 shows the temporal evolution of the radial distribution of the current density where the height along the vertical axis represents the value of the current density along the $-z$ axis ($-j_z$). The current profile is not so largely changed from the equilibrium profile during the linear phase of the kink instability ($t \leqslant 80t_A$). The negative current is observed to form and grow in the vicinity of the geometrical axis as the helical twisting becomes tighter in the nonlinear phase. The absolute value of the current density at the geometrical axis becomes maximum at $t \approx 120t_A$. It is worthy to note that this period coincides with the time when the second relaxation starts. In other words, the second relaxation starts when the reconnection current created by the helical twisting of the flux tube becomes larger than a critical value. The critical value may be determined by the equation where the reconnection rate is balanced with the formation rate of the reconnection current.[18] The reconnection process of the magnetic field lines brings the system to an axisymmetric state, as was seen in the right-bottom panel of Fig. 6. It is concluded that the second relaxation is the transition from

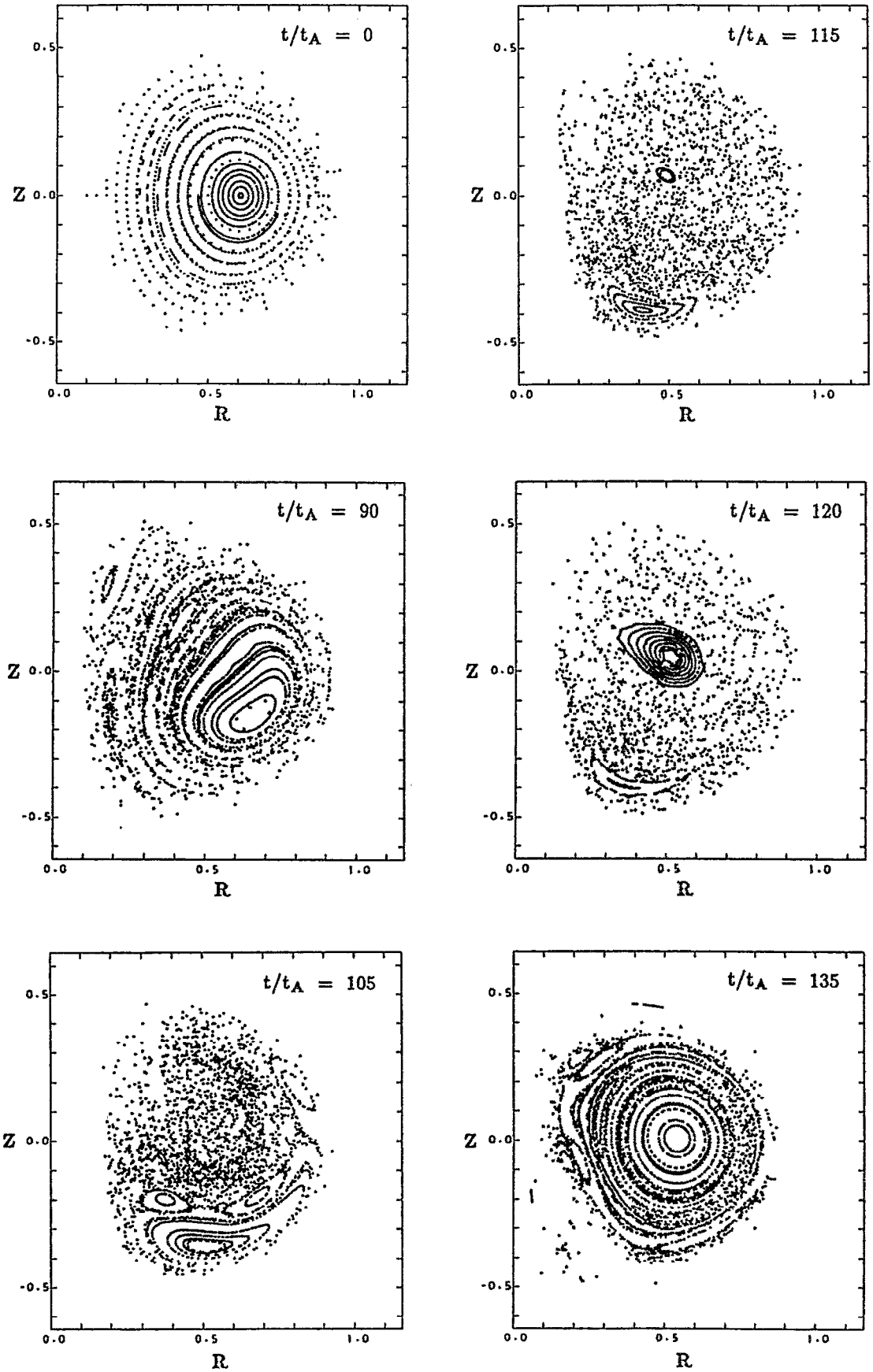


FIG. 5. The Poincaré plots of magnetic field on the poloidal plane ($\phi = 0$) at six different times for case A where six panels correspond to the Poincaré plots at $t = 0, 90t_A, 105t_A, 115t_A, 120t_A$, and $135t_A$, respectively.

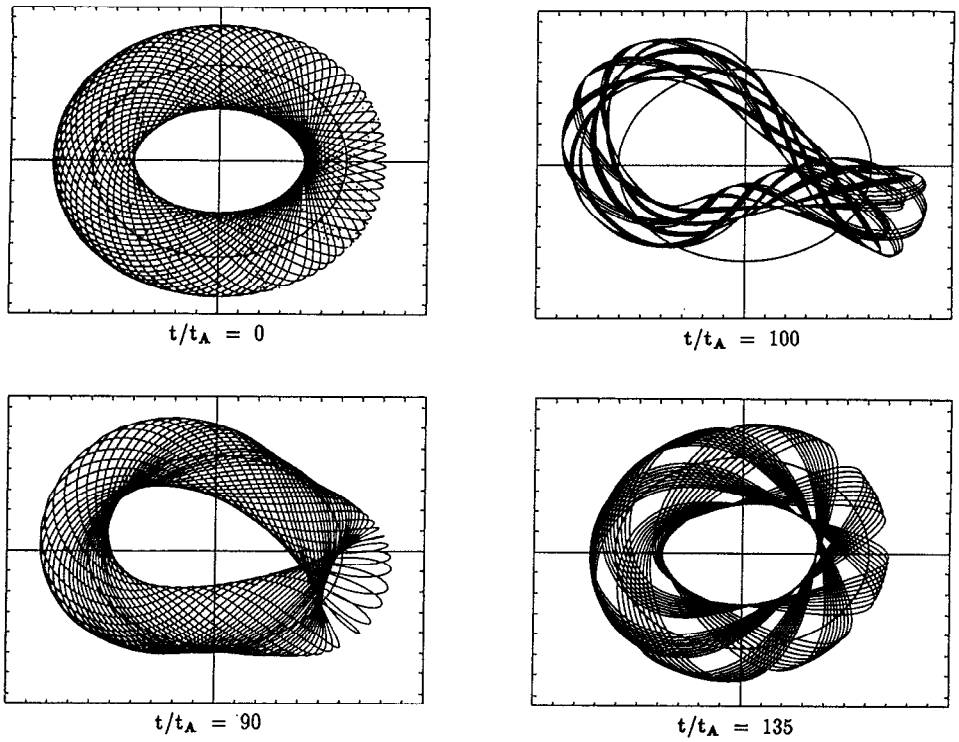


FIG. 6. Three-dimensional display of the magnetic field line at $t = 0$ (left top), $t = 90t_A$ (left bottom), $t = 100t_A$ (right top), and $t = 135t_A$ (right bottom) for case A.

the $n = 2$ helical state to the axisymmetric state through the driven magnetic reconnection.[2]

According to Taylor's hypothesis[4] the minimum energy state is the force-free state with a spatially uniform coefficient $\lambda [\equiv (\mathbf{j}\cdot\mathbf{B})/(\mathbf{B}\cdot\mathbf{B})]$. From this standpoint let us examine the behavior of the spatial distribution of the coefficient $\lambda$ in the relaxation process. Figure 8 shows the perspective diagrams of the distribution of $\lambda$ in the $(r,z)$ plane at $t = 0$, $t = 80t_A$, $t = 120t_A$, and $t = 150t_A$ for case A where the height along the vertical axis normal to the $(r,z)$ plane represents the value of $\lambda$ averaged over the toroidal angle, and both the distributions in the vicinity of the geometrical axis (left side of each panel) and near the boundary surface are excluded from the figure for clarity. The initial distribution is approximately spatially flat except the periphery region, i.e., this profile is very close to the force-free one with minimum energy. As time elapses, the spatial distribution with a peak in the plasma center is gradually formed in accordance with the current peaking ($t = 80t_A$). The nonlinear growth of the kink instability smooths out the peaked distribution and thus a spatially flat distribution is realized at $t = 120t_A$. That is, the kink instability plays a role to adjust the deviation of the magnetic profile created by the resistive process to the force-free one with a minimum energy. Because the resistivity is fixed to be spatially hollow, the peaked distribution grows up again after the second relaxation takes place ($t = 150t_A$).

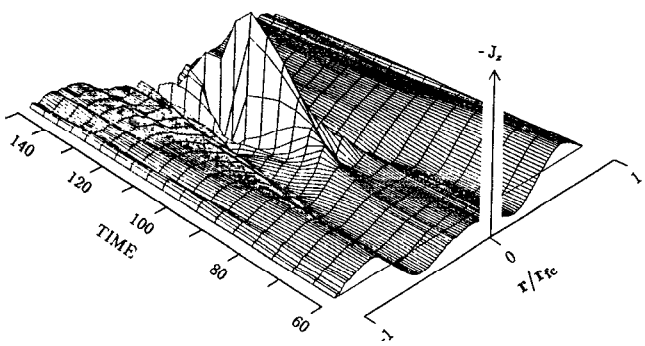


FIG. 7. Temporal evolution of the radial distribution of the current density for case A where the height along the vertical axis represents the value of the current density along the $-z$ axis ($-j_z$).

### B. Flux conversion

As was shown above, the relaxation mechanism in the second relaxation phase is quite different from that in the first relaxation phase. The temporal behaviors of the toroidal magnetic flux and the poloidal magnetic flux exhibit a typical difference between the first and the second relaxation. Figure 9 shows (a) the temporal evolutions of the total toroidal flux (solid line) and the total poloidal flux (dotted line), and (b) that of the ratio of the negative toroidal flux to the total toroidal flux where the flux curves are drawn in a normalized unit. The total poloidal flux begins to decrease just after the first relaxation starts ($t > 80t_A$), while the total toroidal flux remains almost constant until the second relaxation starts ($t > 120t_A$). The negative toroidal flux grows in the nonlinear saturation phase ($80t_A < t < 120t_A$) and dissipates rapidly as soon as the system comes into the second relaxation phase. Both of the growth curves become flat after the second relaxation. A similar result was derived for the low-$q$ simulation carried out by Katayama and Katsurai.[12]

There are two mechanisms that can lead to a decrease in the total poloidal flux. The first one is the resistive dissipation. The poloidal field is distributed with a peak at an inter-

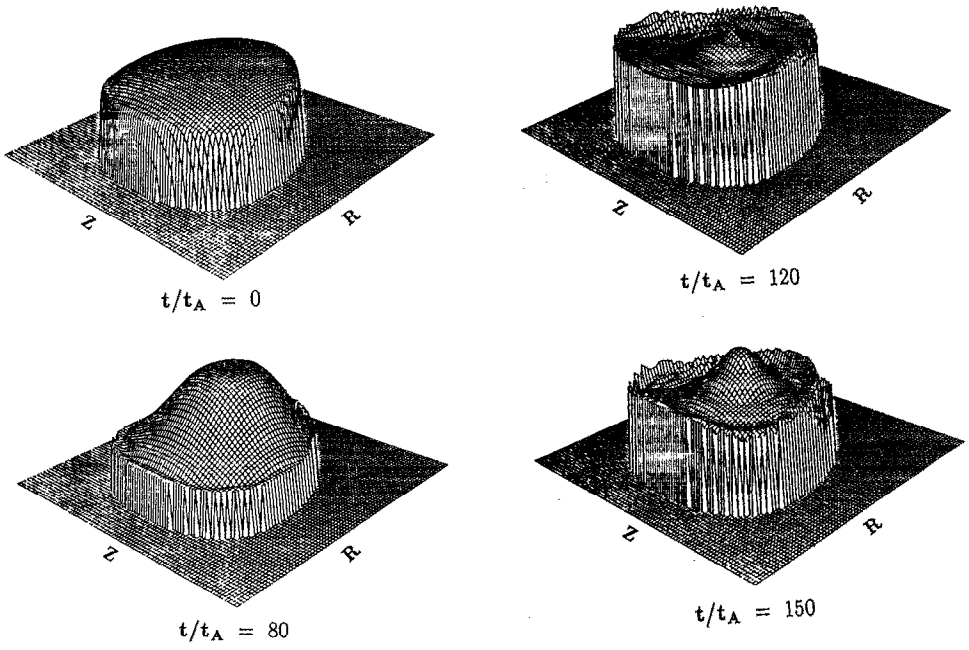


FIG. 8. Perspective diagrams of $\lambda$ in the $(r,z)$ plane at $t = 0$, $t = 80t_A$, $t = 120t_A$, and $t = 150t_A$ for case A where the height along the vertical axis normal to the $(r,z)$ plane represents the value of $\lambda$ averaged over the toroidal angle.

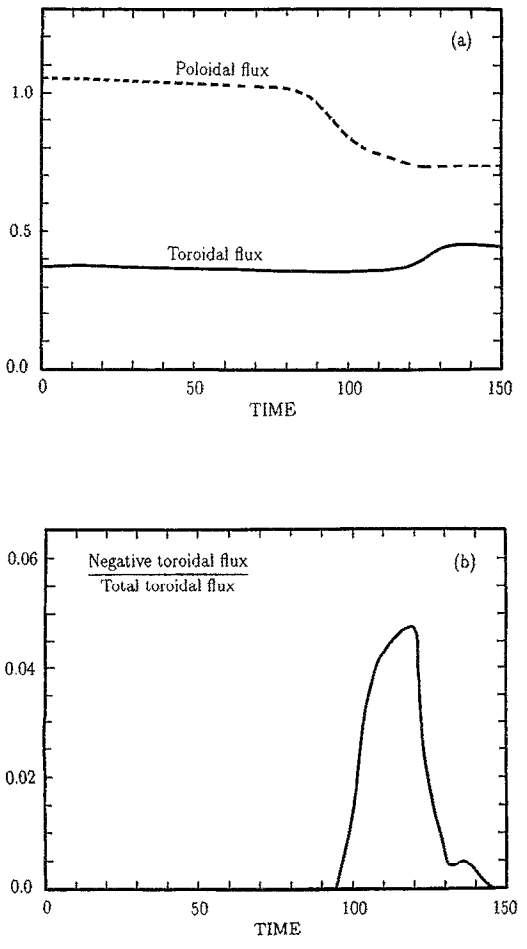


FIG. 9. Temporal evolutions of (a) the total toroidal flux (solid line) and the total poloidal flux (dotted line), and (b) the ratio of the negative toroidal flux to the total toroidal flux, where the flux curves are drawn in a normalized unit.

mediate plasma region while the toroidal field is distributed with a peak at the magnetic axis. Since the resistivity has a hollow profile, the plasma movement toward the conducting wall in the first relaxation leads mainly to resistive dissipation of the poloidal field. The second mechanism is the conversion of the poloidal flux to the toroidal flux via magnetic reconnection.

Let us consider the conversion mechanism by using the schematic model illustrated in Fig. 10. Suppose that two poloidal flux tubes which are located symmetrically around the $z$ axis are forced to deform by the $n = 2$ helical twisting (top panel). The helical twist force lays down the poloidal flux tubes on the plane perpendicular to the $z$ axis in such a way that the directions of the magnetic field lines across the $z$ axis become opposite to each other. This process corresponds to the first relaxation. Since the lying tubes do not have any poloidal flux, the total poloidal flux decreases as a consequence of the helical twisting in the first relaxation. The lying tubes form a reconnection current along the $-z$ axis, as is seen in the middle panel of Fig. 10. It is important to note that the negative toroidal field appears in the vicinity of the $z$ axis while a net amount of the toroidal flux is unchanged at this stage. This can explain the simulation result that the total toroidal flux remains almost constant until the second relaxation starts in spite of the increase of the negative toroidal flux (see Fig. 9). In the second relaxation phase magnetic reconnection takes place at the $z$ axis and it combines two lying flux tubes into one toroidal flux tube that has a net toroidal flux. This process leads not only to elimination of the negative toroidal flux component, but also to the increase of the total amount of the toroidal flux. In this way the behaviors of the poloidal flux and the toroidal flux can be explained without any inconsistency by this simple model illustrated in Fig. 10. Thus, it is concluded that the flux conversion of the poloidal flux to the toroidal flux is realized through successive operations of two processes, i.e., helical

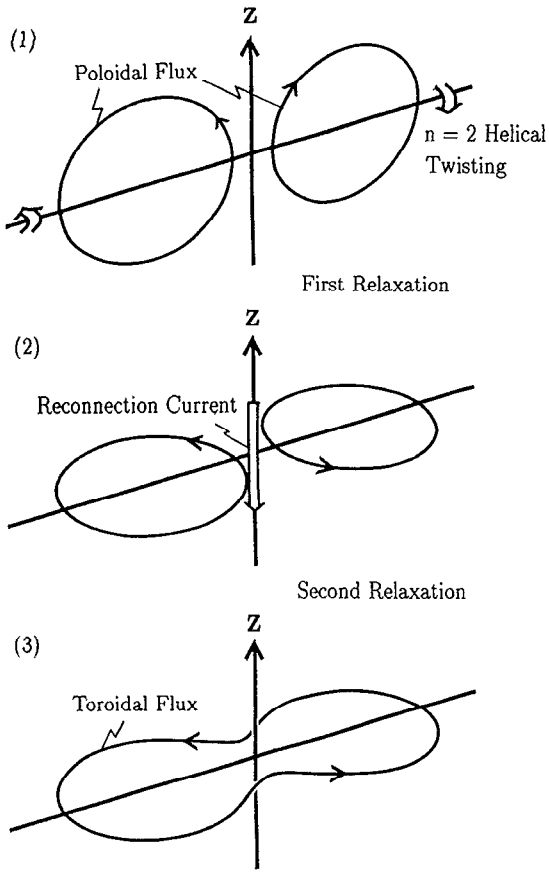


FIG. 10. Schematic diagram of flux conversion mechanism. (1) Two poloidal flux tubes are located symmetrically around the $z$ axis. In the first relaxation the $n = 2$ helical twisting lays down the poloidal flux tubes on the plane perpendicular to the $z$ axis. (2) The reconnection current along the negative $z$ axis is formed and the poloidal flux becomes zero. The toroidal field appears locally, but a net amount of the toroidal flux is zero at this stage. Magnetic reconnection takes place at the $z$ axis in the second relaxation. (3) Consequently, two lying flux tubes are combined into one toroidal flux tube which has a net toroidal flux.

twisting in the first relaxation phase and magnetic reconnection in the second relaxation phase.

### C. Resistivity profile

We have carried out the simulation run by assuming that the resistivity profile is independent of time for case A. It is natural to expect that the spatial profile of the resistivity is largely altered in the nonlinear phase because the flow created by the kink instability carries the hot plasma in the central region to the periphery region. This change may affect the behaviors of the physical quantities in the relaxation process. In order to check this effect we carry out another simulation run in which the resistivity with an ellipsoid profile is used [see Fig. 2(b)]. The parameters are listed in case B of Table I. Note that the resistivity profile in the vicinity of the geometrical axis is most significantly changed from that for case A. This simulation starts from the simulation data at $t = 80t_A$ for case A and is terminated at $t = 150t_A$. The results are displayed in Fig. 11 where the solid, dashed, and dotted lines represent the temporal evolutions of the total

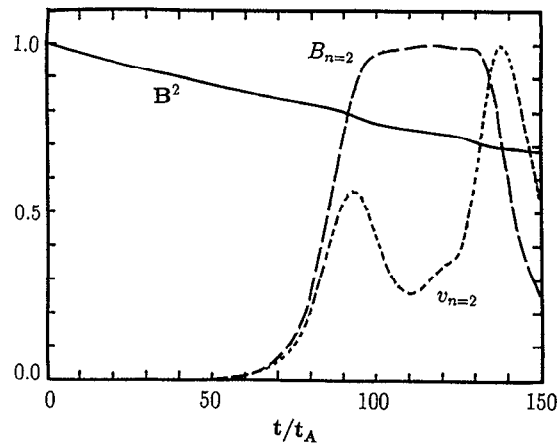


FIG. 11. Same figure as Fig. 3 for case B where the resistivity with an ellipsoid profile is used.

energy, the $n = 2$ mode amplitude of the magnetic field, and that of the flow velocity, respectively. Let us compare the results with those shown in Fig. 3. Because the kink instability is an ideal process caused only by the spatial structure of the magnetic field, the first relaxation is hardly affected by the change of the resistivity profile. The duration of the nonlinear saturation phase becomes longer and the start of the second relaxation is delayed. Recall the fact that the second relaxation starts when the reconnection current created by the helical twisting becomes larger than a critical value. This indicates that the formation of the reconnection current in the vicinity of the geometrical axis is the resistive process and thus more time is necessary for the reconnection current to grow to the critical value for case B.

### D. Dependence on the toroidal mode

The reconnection process plays a key role on the transition from the helically symmetric state to the axially symmetric state in the second relaxation phase. Incidentally we observe that the $n = 1$ and $n = 3$ modes grow rapidly near the geometrical axis just before the second relaxation starts. The same phenomenon was observed in the CTCC-I experiment.[9] In order to clarify the relation between the reconnection process and these modes we carry out two simulation runs, i.e., case C where the $n = 3$ mode is excluded from the simulation and case D where the $n = 1$ mode is excluded from the simulation. Though the simulation code used is not the Fourier code, we carry out the Fourier transformation of the simulation data once every ten time steps ($\simeq 0.04t_A$) and reset the amplitude of the assigned mode equal to zero. These simulation runs start with the data at $t = 80t_A$ for case A. Figure 12 shows the temporal evolution of the kinetic energy for case A (solid line), case C (dotted line), and case D (dashed line) where the amplitude is normalized by the maximum value of all. The kinetic energy in the first relaxation phase evolves in the same way for three cases. This is due to the fact that the first relaxation is caused by the growth of the $n = 2$ ideal kink mode and the $n = 1$ and $n = 3$ modes do not play any role on the first relaxation phenomenon, as was

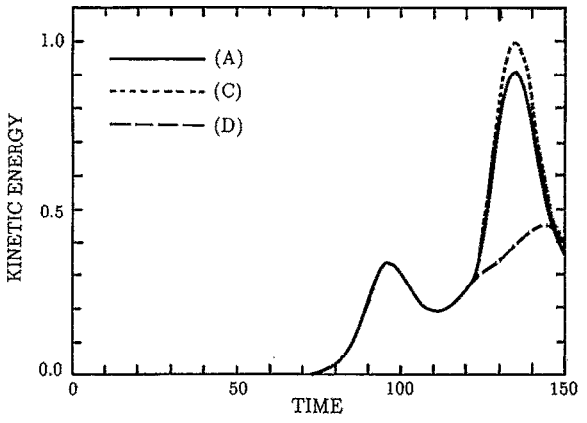


FIG. 12. Temporal evolutions of the kinetic energy for case A (solid line), case C (dotted line), and case D (dashed line) where the amplitude is normalized by the maximum value of all.

seen in Fig. 4. On the other hand, the second relaxation reveals a quite different feature, i.e., there is not any clear peak of the kinetic energy for case D while the kinetic energy for case C behaves in the same way as for case A. In other words, there is not any clear period corresponding to the second relaxation phase in the simulation run without the $n = 1$ mode. This suggests that the existence of the $n = 1$ mode is necessary for the complete performance of the second relaxation which is controlled by magnetic reconnection.

Figure 13 shows the temporal evolution of the current density at the geometrical axis for the same cases as Fig. 12. The reconnection current increases gradually as a result of the helical twisting of the flux tube in the nonlinear saturation phase ($100t_A < t < 120t_A$). For cases A and C we can observe evidence that the second relaxation starts at the period ($t = 120t_A$) when the reconnection current reaches a critical value. The energy stored in the twisted flux tube is released through magnetic reconnection and it forms the second peak of the kinetic energy, as was seen in Fig. 12. Consequently, the current density at the geometrical axis decreases as the second relaxation proceeds ($120t_A < t < 140t_A$). On the other hand, the reconnection

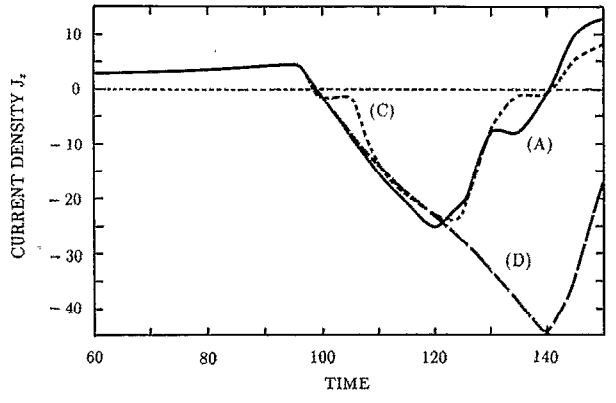


FIG. 13. Temporal evolution of the current density at the geometrical axis for the same cases as Fig. 12.

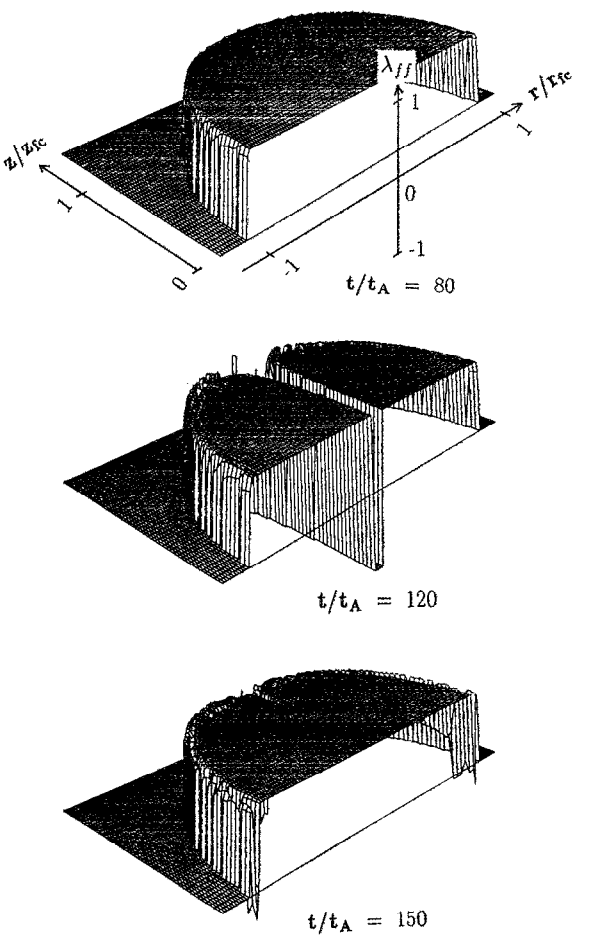


FIG. 14. Temporal evolution of the force-free parameter $\lambda_{ff}$ for case C where three panels show the perspective views of $\lambda_{ff}$ in the upper half ($z > 0$) of the poloidal cross section at $t = 80t_A$ (top), $t = 120t_A$ (middle), and $t = 150t_A$ (bottom), respectively.

current for case D continues to increase after it reaches a critical value for cases A and C. That is, neither the decrease of the current density at the geometrical axis nor the rapid growth of the kinetic energy showing the efficient operation of magnetic reconnection appear for the simulation run without the $n = 1$ mode.

Let us consider the role of the $n = 1$ mode on the magnetic reconnection process in the second relaxation. First, recall the mathematical condition that each component of a vector has the structure described by only a toroidal mode at the geometrical axis in the cylindrical coordinates, i.e., the axial component has the $n = 0$ structure while the radial and azimuthal components have the $n = 1$ structure. The $n = 2$ helical twisting does not lead to the formation of the magnetic field or the current density with the $n = 1$ structure because of its $n = 2$ symmetry. Thus, both the magnetic field and the current density have only an axial component with the $n = 0$ structure on the axis. In other words, the profile satisfying the force-free condition $\mathbf{J} \times \mathbf{B} = 0$ is formed at the geometrical axis as a result of the helical twisting. Figure 14 shows the temporal evolution of the force-free parameter $\lambda_{ff}$ for case C where three panels show the perspective views of

the parameter $\lambda_{ff}$ ($\equiv \mathbf{J}\cdot\mathbf{B}/|\mathbf{J}||\mathbf{B}|$) in the upper half ($z>0$) of the poloidal cross section at $t=80t_A$ (top), $t=120t_A$ (middle), and $t=150t_A$ (bottom), respectively. Though the whole system is slowly modified from the initial equilibrium, the magnetic field continues to have a configuration very close to the force-free one of $\lambda_{ff}=1$ during the linear phase (top). The helical twisting of the flux tube in the nonlinear phase creates another force-free configuration of $\lambda_{ff}=-1$ in the vicinity of the geometrical axis (middle). It is important to note that two different force-free states exist in the nonlinear phase simultaneously. The force-free state of $\lambda_{ff}=-1$ disappears after the second relaxation phase (bottom). This phenomenon corresponds to the disappearance of the reconnection current sustaining the reversed field. There are two processes through which the current profile is changed in the MHD plasma, i.e., the diffusion process and the reconnection process. The diffusion of the magnetic field takes place in a resistive time scale that is much longer than an MHD time scale. In the reconnection process the magnetic flux is carried away from the reconnection point by the dynamical flow created by the $\mathbf{J}\times\mathbf{B}$ force and hence the current profile is changed in the short time scale comparable to the MHD time scale. The intermediate state of $1>\lambda_{ff}>-1$, in which the relation $\mathbf{J}\times\mathbf{B}\neq 0$ holds, is required for the transition from the $\lambda_{ff}=-1$ state to the $\lambda_{ff}=1$ state in a short time scale. It is clear that the $n=1$ mode is necessary to describe the $|\lambda_{ff}|\neq 1$ state at the geometrical axis. Therefore it is concluded that the existence of an $n=1$ mode with a sufficiently large amplitude is indispensable for the complete performance of magnetic reconnection in the second relaxation. The $n=3$ mode grows as a result of the nonlinear coupling between the $n=1$ mode and the $n=2$ mode, but this mode does not play any essential role in the reconnection process. These conclusions are quite different from the results of the numerical simulation carried out by Sgro *et al.*[11] or that done by Ono and Katsurai.[13]

## IV. SUMMARY AND DISCUSSIONS

We have examined the whole relaxation process of a spheromak plasma in a flux conserver from an initial current peaking phase through the final force-free state by making use of the three-dimensional full MHD simulation and have clarified the physical mechanism of the stepwise relaxation. The main results are summarized as follows.

(1) The current peaking near the magnetic axis proceeds in the resistive time scale due to the hollow resistivity profile. When an initial force-free profile changes to a low-$q$ profile of $q<0.5$, the stepwise relaxation of the magnetic energy is triggered by excitation of the $m=1/n=2$ ideal kink mode. The stepwise relaxation consists of four temporal phases, i.e., the linear phase, the first relaxation phase, the nonlinear saturation phase, and the second relaxation phase.

(2) In the linear phase both the $n=2$ flow mode and the $n=2$ magnetic field mode created by the helical kink instability grow with the same rate, which is nearly equal to $0.13/t_A$. As the amplitude of the $n=2$ kink mode increases, the magnetic flux tube is helically deformed in a way that one would twist a candy wrapper. The flow created by the helical kink instability carries the hot plasma in the central region to the periphery region with a relatively large resistivity. Therefore, this movement results in a rapid dissipation of magnetic energy in the first relaxation phase.

(3) The $n=2$ helical structure is nonlinearly sustained for a while after the growth of the helical kink instability is stopped. The magnetic island surrounding the magnetic axis is deformed in a fairly crescent shape. The helical twisting of the flux tube forms the reconnection current at the contact point which is located on the geometrical axis. The reconnection current develops gradually to create a reversed toroidal field near the geometrical axis. This period corresponds to the nonlinear saturation phase.

(4) When the reconnection current becomes larger than a critical value, magnetic reconnection takes place at the geometrical axis and the dynamical flow created by the $\mathbf{J}\times\mathbf{B}$ force carries away the reconnected magnetic flux from the reconnection point. Consequently, the helical twisting is relaxed and the axially symmetric force-free state is realized again in the plasma. This is the second relaxation. This process requires the existence of an $n=1$ mode with a sufficiently large amplitude.

(5) The flux conversion from the poloidal flux to the toroidal flux is realized through the two processes of helical twisting in the first relaxation and magnetic reconnection in the second relaxation.

(6) The resistivity dependence of the relaxation phenomena is also examined by changing the spatial distribution of the resistivity. It is found that the duration of the nonlinear saturation phase becomes longer and the start of the second relaxation is delayed when the simulation is carried out for the resistivity profile with a smaller value near the geometrical axis.

In this paper we made several assumptions to examine the whole process of the stepwise relaxation by the three-dimensional full MHD simulation code with a fourth-order accuracy. Before concluding this paper, let us discuss the plausibility of these assumptions.

The resistivity profile was assumed to be independent of time. The resistivity plays three important roles on the stepwise relaxation. The first role is to change the stable force-free configuration to an unstable configuration against the kink mode through the peaking of the current profile. The second one is to cause the rapid dissipation of magnetic energy in the first relaxation phase. These phenomena are caused essentially by the hollow spatial profile in which the resistivity at the periphery is larger than that in the center region. The third role is to change magnetic topology through magnetic reconnection. The reconnection rate is almost independent of the absolute value of the resistivity for the driven reconnection.[2,18] However, the formation speed of the reconnection current in the nonlinear saturation phase depends on the resistivity near the geometrical axis, as was seen in Sec. III C. Therefore, it is plausible that the temporal change of the resistivity profile exerts influence on the phenomena in the nonlinear saturation phase. This result is considered to correspond to the experimental fact that the saturation of the $n=2$ mode was not observed in the late phase of the discharge.[9]

We started the simulation from an equilibrium profile that was close to the critical profile of $q_{axis} = 0.5$. The purpose of this paper is to examine the whole process of the stepwise relaxation in the system with two different time scales, i.e., the MHD time scale and the resistive diffusion time scale, by means of the full MHD simulation code. For this we need to carry out the simulation over a large number of time steps. Especially, the initial current peaking phase and the growing phase of a perturbation from a numerical noise level to a nonlinear level are the major parts. Because the accumulation of numerical error increases in proportion to the number of time steps, the total number of time steps should be kept less than a permissible value. The number of time steps needed to obtain physically reliable simulation data is restricted within several tens of thousands when the MHD simulation code with fourth-order accuracy is used. The physical period of $150t_A$ corresponds to about 40 000 time steps for the case of the MHD simulation code used in this paper. There are two ways to reduce the number of time steps without losing the reliability. The first way is to make the value of resistivity larger and to contract the difference between the resistive time scale and the MHD time scale. This method sometimes makes it impossible to identify a physical process controlling the phenomenon among various processes with different time scales. Thus, we did not use this method. Instead, we relied on the second way in which we exclude part of the natural phenomena, which is not essential to clarify the physical process, from the simulation and shorten the physical time of the simulation. In the real experiment[9] the initial $q_{axis}$ is close to 0.6. However, based on our premise that the current peaking phase from $q_{axis} = 0.6$ to $q_{axis} = 0.5$ must be controlled by the same mechanism as that from $q_{axis} = 0.524$ to $q_{axis} = 0.5$, we adopted the initial equilibrium profile with $q_{axis} = 0.524$ rather than 0.6.


## ACKNOWLEDGMENT

The authors are grateful to Professor Kenji Watanabe for his continuous interest in this work.



[1] R. Horiuchi and T. Sato, Phys. Rev. Lett. **55**, 211 (1985); Phys. Fluids **29**, 1161, 4174 (1986).
[2] T. Sato and T. Hayashi, Phys. Fluids **22**, 1189 (1979).
[3] D. J. Campbell, L. D. Gill, C. W. Gowers, J. A. Wesson, D. V. Bartlett, C. H. Best, S. Coda, A. E. Costley, A. Edwards, S. E. Kissel, R. M. Niestadt, H. W. Piekaar, R. Prentice, R. T. Ross, and B. T. D. Turning, Nucl. Fusion **26**, 1085 (1986).
[4] J. B. Taylor, Phys. Rev. Lett. **33**, 1139 (1974).
[5] J. M. Finn and A. Reiman, Phys. Fluids **25**, 116 (1984); G. W. Hart, A. Janos, D. D. Meyerhofer, and M. Yamada, *ibid.* **29**, 1994 (1986).
[6] W. N. Rosenbluth and M. N. Bussac, Nucl. Fusion **19**, 489 (1979); J. H. Hammer, *ibid.* **21**, 488 (1981); A. Bondeson, G. Marklin, Z. G. An, H. H. Chen, Y. C. Lee, and C. S. Liu, Phys. Fluids **24**, 1682 (1981).
[7] T. Hayashi and T. Sato, Phys. Fluids **27**, 778 (1984); T. Hayashi, T. Sato, F. Wysocki, D. D. Meyerhofer, and M. Yamada, J. Phys. Soc. Jpn. **54**, 4172 (1985).
[8] T. Hayashi and T. Sato, Phys. Fluids **28**, 3654 (1985): T. J. Jarboe, I. Henins, A. R. Sherwood, C. W. Barnes, and H. W. Hoida, Phys. Rev. Lett. **51**, 39 (1983).
[9] T. Uyama, Y. Honda, M. Nagata, M. Nishikawa, A. Ozaki, N. Satomi, and K. Watanabe, Nucl. Fusion **27**, 799 (1987); Y. Honda, Y. Kato, N. Satomi, M. Nishikawa, and K. Watanabe, J. Phys. Soc. Jpn. **57**, 1273 (1988).
[10] S. O. Knox, C. W. Barnes, G. J. Marklin, T. R. Jarboe, J. Hennins, H. W. Hoida, and B. L. Wright, Phys. Rev. Lett. **56**, 842 (1986).
[11] A. G. Sgro, A. A. Mirin, and G. Marklin, Phys. Fluids **30**, 3219 (1987).
[12] K. Katayama and M. Katsurai, Phys. Fluids **29**, 1939 (1986).
[13] Y. Ono and M. Katsurai, Nucl. Fusion **31**, 233 (1991).
[14] R. Horiuchi and T. Sato, Phys. Fluids B **1**, 581 (1989).
[15] T. Sato, Y. Nakayama, T. Hayashi, K. Watanabe, and R. Horiuchi, Phys. Rev. Lett. **63**, 528 (1989).
[16] K. Watanabe and T. Sato, J. Geophys. Res. **95**, 75 (1990).
[17] J. L. Johnson, H. E. Dalhed, J. M. Greene, R. C. Grimm, Y. Y. Hsieh, S. C. Jardin, J. Manickam, M. Okabayashi, R. G. Storer, A. M. M. Todd, D. E. Voss, and K. E. Weimer, J. Comput. Phys. **32**, 212 (1979).
[18] T. Sato, R. Horiuchi, and K. Kusano, Phys. Fluids B **1**, 255 (1989); T. Sato, T. Hayashi, K. Watanabe, R. Horiuchi, M. Tanaka, N. Sawairi, and K. Kusano, Phys. Fluids B **4**, 450 (1992).